Supplementary information

Dual-MOF-Derived Ni@Fe-Based Core–Shell Heterostructures as Trifunctional Catalysts for Methanol Valorization-Coupled H_2 Production via Hybrid Water Electrolysis

Apurba Borah,[a] Sayan Das,[a] Vishakha Singh[a] and Gaddam Rajeshkhanna*[a]

[a]Department of Chemistry, National Institute of Technology Warangal, Hanumakonda-506004, India. *E-mail: grkhanna@nitw.ac.in

1. Experimental section

1.1. Material used. $Ni(NO_3)_2.6H_2O$, Terephthalic acid ($C_6H_4(CO_2H)_2$), $K_3[Fe(CN)_6]$, KOH (85%), HCl (~35%), 2,2-dimethylformamide (DMF) and acetone were commercially obtained from FINAR. $NaH_2PO_2.H_2O$ was commercially obtained from Spectrochem. RuO_2 and Pt/C (20 wt%) were commercially obtained from Merck Sigma-Aldrich. Ni foam (NF) was commercially obtained from Vritra Technologies. Double-deionized (DI) H_2O and ethanol were employed for cleaning and synthesis.

1.2. Synthesis of electrocatalyst materials. Ni foam (NF) measuring 2×4 cm^2 underwent a cleaning process involving sonication in aqueous 3 M HCl solution for 10 minutes to effectively eliminate the oxidized surface layer, subsequently followed by multiple washings with DI H_2O and acetone. The cleaned NF was dried for 1 hour at 35 °C using hot air oven. The dried NF was placed inside a Teflon-lined stainless-steel autoclave of 50 mL capacity containing 1:1 solution of 20 mL DI H_2O and 20 mL DMF, in which 1 mmol $Ni(NO_3)_2.6H_2O$ and 1 mmol terephthalic acid (TPA) were dissolved. The autoclave was sealed and heated for 12 h at 120 °C in hot air oven, followed by cooling naturally to room temperature. The mint blue colored material deposited on NF was named Ni-TPA/NF, which was repeatedly washed

with DI H_2O and ethanol followed by drying at 60 °C for 8 hours. The Ni-TPA/NF was calcined in air for 2 h at 500 °C with a ramp rate of 3 °C min^{-1} to get black colored NiO/NF. Another piece of synthesized Ni-TPA/NF was kept immersed in 0.05 M aqueous solution of $K_3[Fe(CN)_6]$ for 12 h at ambient condition to allow the growth of Prussian Blue (PB) MOF, which is denoted as Ni-TPA@PB/NF. The material was washed and dried following same procedure. The dark moss green colored Ni-TPA@PB/NF was converted to the corresponding oxide by calcining in air at 500 °C for 2 h with a ramp rate of 3 °C min^{-1}. The obtained reddish brown colored material is denoted as NiO@Fe_3O_4/NF. Similarly, Ni-TPA@PB/NF was converted to corresponding phosphide by heating under flowing N_2 gas at 500 °C for 2 h with 3 °C min^{-1} ramp rate in presence of $NaH_2PO_2.H_2O$ as the phosphating agent in the upstream position of flowing N_2 gas. The obtained black colored material is denoted as Ni_2P@Fe_2P/NF.

To understand the necessity of the dual MOF-precursor for Ni_2P@Fe_2P/NF, a control experiment was conducted. In the control experiment, a precleaned NF of 2 × 4 cm^2 dimension was placed inside a 50 mL Teflon-lined stainless-steel autoclave with a 40 mL aqueous solution of 0.2 mmol $Fe(NO_3)_3.9H_2O$, 1 mmol $Ni(NO_3)_2.6H_2O$, 4 mmol urea, and 4 mmol NH_4F. The as-prepared aqueous solution with the immersed NF was hydrothermally treated for 12 h at 120 °C in hot air oven using 50 mL capacity Teflon-lined stainless-steel autoclave. The obtained material-coated NF was named as NiFe-OH/NF. The as-obtained NiFe-OH/NF was phosphidized following the same procedure as described above to get the non-MOF-derived Ni_2P-Fe_2P/NF.

1.3. RuO_2 and Pt/C electrode fabrication. 15 mg RuO_2 and 15 mg Pt/C (Pt content of 20 wt %) were placed into two distinct glass vials. A homogenous mixture was achieved by introducing a solution comprised of 480 µL deionised water, 480 µL isopropyl alcohol and 40 µL 5 wt% nafion solution into the RuO_2 and Pt/C sample vials, followed by sonication for 30

minutes. The resultant catalyst inks were uniformly drop-cast onto a 1×1 cm^2 NF substrate and subsequently subjected to drying at 60 °C for 8 hours. The quantity of material deposited on NF in each case approximates 9 mg cm^{-2}.

1.4. Physicochemical characterization. Powder X-ray diffraction (PXRD) patterns were recorded utilizing Cu Kα radiation with a wavelength of 1.54 Å using XPERT-PRO diffractometer instrument. Fourier-transform infrared (FT-IR) spectroscopy was conducted using BRUKER ALPHA II instrument in the wavenumber window of 400 to 4000 cm^{-1}. Field emission scanning electron microscopy (FESEM) images were recorded using Thermo Fisher FEI-Quanta 250 FEG instrument. Brunauer-Emmett-Teller (BET) analysis was executed using a Quantachrome® Autosorb iQ instrument. High-resolution transmission electron microscopy (HRTEM) was executed utilizing a Tecnai G2 20 TWIN instrument. X-ray photoelectron spectroscopy (XPS) was performed using a Thermo Fisher SCIENTIFIC instrument**.**

1.5. Electrochemical measurements. All-electrochemical measurements were conducted using BioLogic Science Instruments (SP-150e) workstation, where a three-electrode configuration was employed for the oxygen evolution reaction (OER) and hydrogen evolution reaction (HER) and a two-electrode configuration was utilized for the overall water electrolysis (OWE) investigations. In the three-electrode configuration, 1 M KOH filled Hg-HgO as reference electrode, graphite rod as counter electrode, and 1 cm^2 area of electrocatalyst-loaded NF with a loading of approximately 9 mg cm^{-2} was employed as the working electrode. In the two-electrode configuration, two identical materials were used as both anode and cathode, forming a symmetrical electrolyser. The measured potentials recorded against Hg-HgO (1M KOH) reference electrode were subsequently converted into reversible hydrogen electrode (RHE) using the conversion equation as follows:[S1]

$$E_{RHE} = E_{Hg-HgO/1\,M\,KOH} + 0.059pH + 0.098\,V \quad \text{(S1)}$$

All the electrochemical performances were conducted in 1 M KOH as electrolyte solution. Initially, 100 cycles of cyclic voltammetry (CV) of the working electrode were conducted at a scan rate of 50 mV s^{-1} to make the electrochemical data more reliable by activating and stabilizing the electrode materials. The LSV (Linear Sweep Voltammetry) curves were recorded at a low scan rate of 2 mV s^{-1} allowing detailed analysis of the electrochemical processes occurring at the electrode surface, providing insights into the kinetics of the reaction.[S2] All the OER, HER, MOR and OWE data are presented without any *iR*-correction. However, the equation for *iR*-correction is:

$$E_{corr} = E_{mea} - iR_{ct} \quad \text{(S2)}$$

where E_{corr} is the *iR*-corrected potential, E_{mea} is the experimentally measured potential, R_{ct} is the charge transfer resistance, and i is the corresponding current.[S3,S4]

The overpotential was calculated by using following equation.[S3]

For OER, $\eta = E_{RHE} - 1.23\ V$ (S3)

For HER, $\eta = E_{RHE} - 0\ V$ (S4)

The Tafel plots were derived from LSV curves to enhance the comprehension of the kinetics associated with the OER and HER through the application of the subsequent equation:[S2]

$$\eta = a\log j + b \quad \text{(S5)}$$

where a defines the Tafel slope, j defines the current density and b is the intercept on the overpotential axis. A quicker reaction speed is linked to a lower Tafel slope, while a slower reaction speed leads to higher Tafel slope values. Exchange current densities (j_0) were calculated using Nyquist plots by the following equation.[S5]

$$j_0 = \frac{RT}{nFR_{ct}} \quad \text{(S6)}$$

where R defines the universal gas constant (8.314 J K^{-1} mol^{-1}), T is reaction temperature (298.15 K), n is the number of electrons transferred (n = 4 for OER, n = 4 for methanol

oxidation to formate, and n = 2 for HER), and R_{ct} is charge transfer resistance obtained from Nyquist plots.[S5] Electrochemical impedance spectroscopy (EIS) was performed at 1.53 V for OER and -0.27 V for HER in the frequency range from 0.01 to 10^6 Hz to obtain the Nyquist plots.

The double-layer capacitance (C_{dl}) was calculated using cyclic voltammetry curves recorded in non-faradic regions at scan rates ranging from 10 to 100 mVs^{-1}. The slope obtained by plotting the difference in capacitive current densities versus scan rates are equal to twice the C_{dl} values. The electrochemical active surface area (ECSA) was calculated using the C_{dl} value by using the following formula:[S3,S4]

$$ECSA = \frac{C_{dl}}{C_s cm^{-2}_{ECSA}} \quad \text{(S7)}$$

where C_s is the specific capacitance, which was assumed to be 0.04 mF cm^{-2} by considering the reported literature for a smooth metal surface.

To evaluate the endurance of the electrocatalyst and the fabricated electrolyzer's applicability, the chronopotentiometry (CP) test was conducted for OER, HER, and OWE at 50 mA cm^{-2} current density for 50 and 70 h test period, respectively.

The faradaic efficiency (FE) of the electrocatalyst for H_2 and O_2 production was calculated by following the equation:[S6]

$$FE\ of\ H_2 = \frac{Experimental\ gas\ production\ in\ mL\ (V_1)}{Calculated\ gas\ production\ in\ mL\ (V_2)} = {V_1}\Big/{\left(\frac{2QV_m}{4F}\right)} \quad \text{(S8)}$$

$$FE\ of\ O_2 = \frac{Experimental\ gas\ production\ in\ mL\ (V_3)}{Calculated\ gas\ production\ in\ mL\ (V_4)} = {V_3}\Big/{\left(\frac{1QV_m}{4F}\right)} \quad \text{(S9)}$$

where Q is the total charge passed through the electrodes, V_m is the molar volume of gas (24.45 L mol^{-1} at 298.15 K and 1 atm), F is the Faraday constant (96,485 C mol^{-1}), the number *4* defines 4 moles of electrons per mole of H_2O, the number *2* defines 2 moles of H_2 per mole of H_2O, and the number *1* defines 1 mole of O_2 per mole of H_2O.

2. Calculation of energy consumption cost for H_2 production per kilogram

Using the conventional (OER + HER) Ni_2P@Fe_2P/NF(±) electrolyzer:

Current applied = 500 mA = 0.5 A

The voltage required to reach 0.5 A = 2.51 V

Rate of H_2 production = 3.43 mL min^{-1}

The time needed for production of 1 kL H_2 gas = 4859.1 h

Power consumption (kL^{-1}) = 0.5 A × 2.51 V × 4859.1 h = 6098.2 W h = 6.0982 kW h

Cost of 1 kL H_2 gas = Power consumption × electricity bill

= 6.0982 kW h × \$0.02/kW h = \$0.12196

Using the conventional (OER + HER) NiO@Fe_3O_4/NF(±) electrolyzer:

Current applied = 500 mA = 0.5 A

The voltage required to reach 0.5 A = 2.62 V

Rate of H_2 production = 3.34 mL min^{-1}

The time needed for production of 1 kL H_2 gas = 4990 h

Power consumption (kL^{-1}) = 0.5 A × 2.62 V × 4990 h = 6536.9 W h = 6.5369 kW h

Cost of 1 kL H_2 gas = Power consumption × electricity bill

= 6.5369 kW h × \$0.02/kW h = \$0.1307

Using the hybrid (MOR + HER) Ni_2P@Fe_2P/NF(±) electrolyzer:

Current applied = 200 mA = 0.2 A

The voltage required to reach 0.2 A = 2.03 V

Rate of H_2 production = 1.52 mL min^{-1}

The time needed for production of 1 kL H_2 gas = 10964.9 h

Power consumption (kL^{-1}) = 0.2 A × 2.03 V × 10964.9 h = 4451.7 W h = 4.4517 kW h

Cost of 1 kL H_2 gas = Power consumption × electricity bill

= 4.4517 kW h × \$0.02/kW h = \$0.089

At 298.15 K temperature and 1 atm pressure, 1 kL H_2 equals to 0.08239 kg. Therefore, the electricity cost for 1 kg of produced H_2 using:

Hybrid (MOR + HER) Ni_2P@Fe_2P/NF(±) electrolyzer is \$1.08,

Conventional (OER + HER) Ni_2P@Fe_2P/NF(±) electrolyzer is \$1.48, and

Conventional (OER + HER) NiO@Fe_3O_4/NF(±) electrolyzer is \$1.59.

3. Mass activity calculation

The mass activity of the materials was calculated by dividing the resulted current densities in the OER LSV by the mass of electrocatalyst deposited on the nickel foam substrate. The deposited mass of electrocatalysts on nickel foam substrate was calculated experimentally.

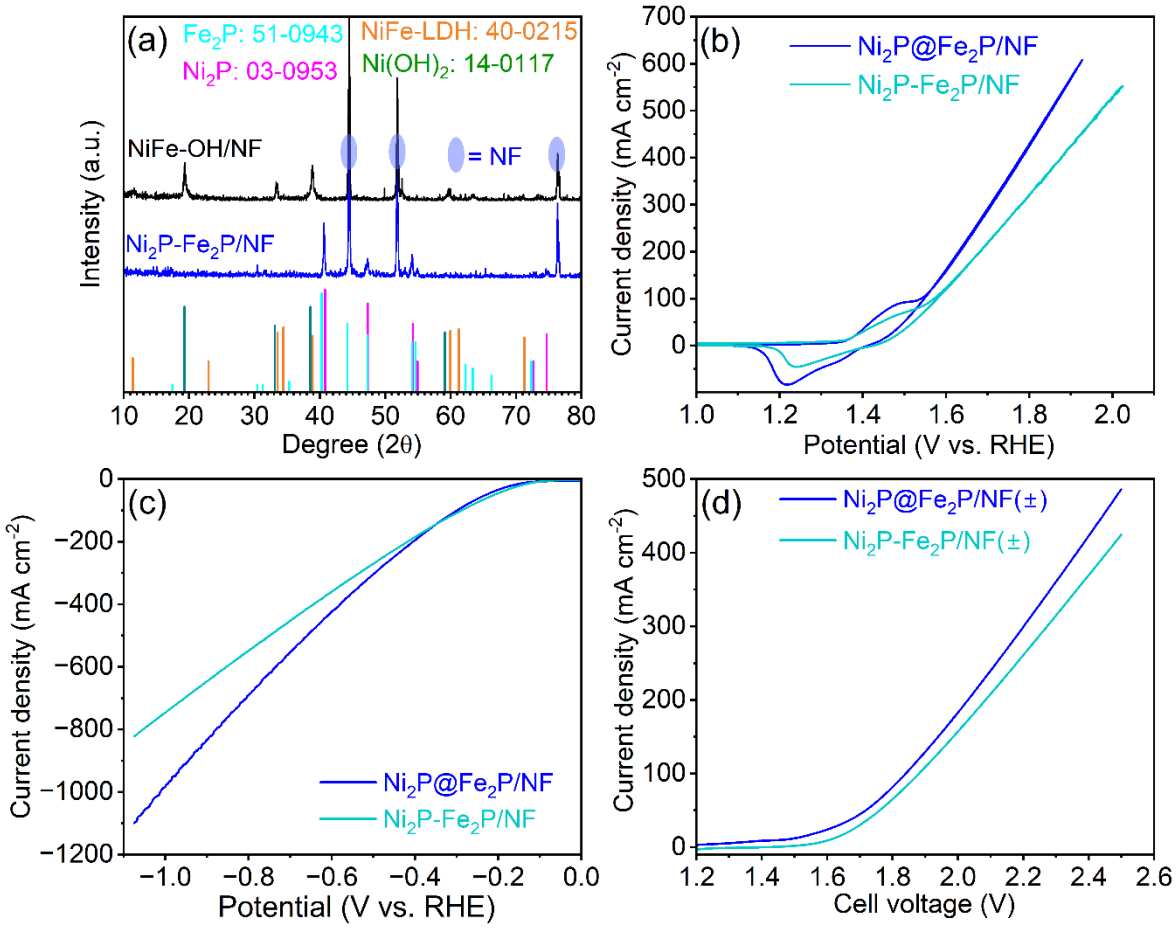

Fig. S1 (a) PXRD patterns of NiFe-OH/NF and Ni_2P-Fe_2P/NF, comparison of (b) OER, (c) HER, and (d) OWE activities of MOF-derived Ni_2P@Fe_2P/NF with non-MOF-derived Ni_2P-Fe_2P/NF.

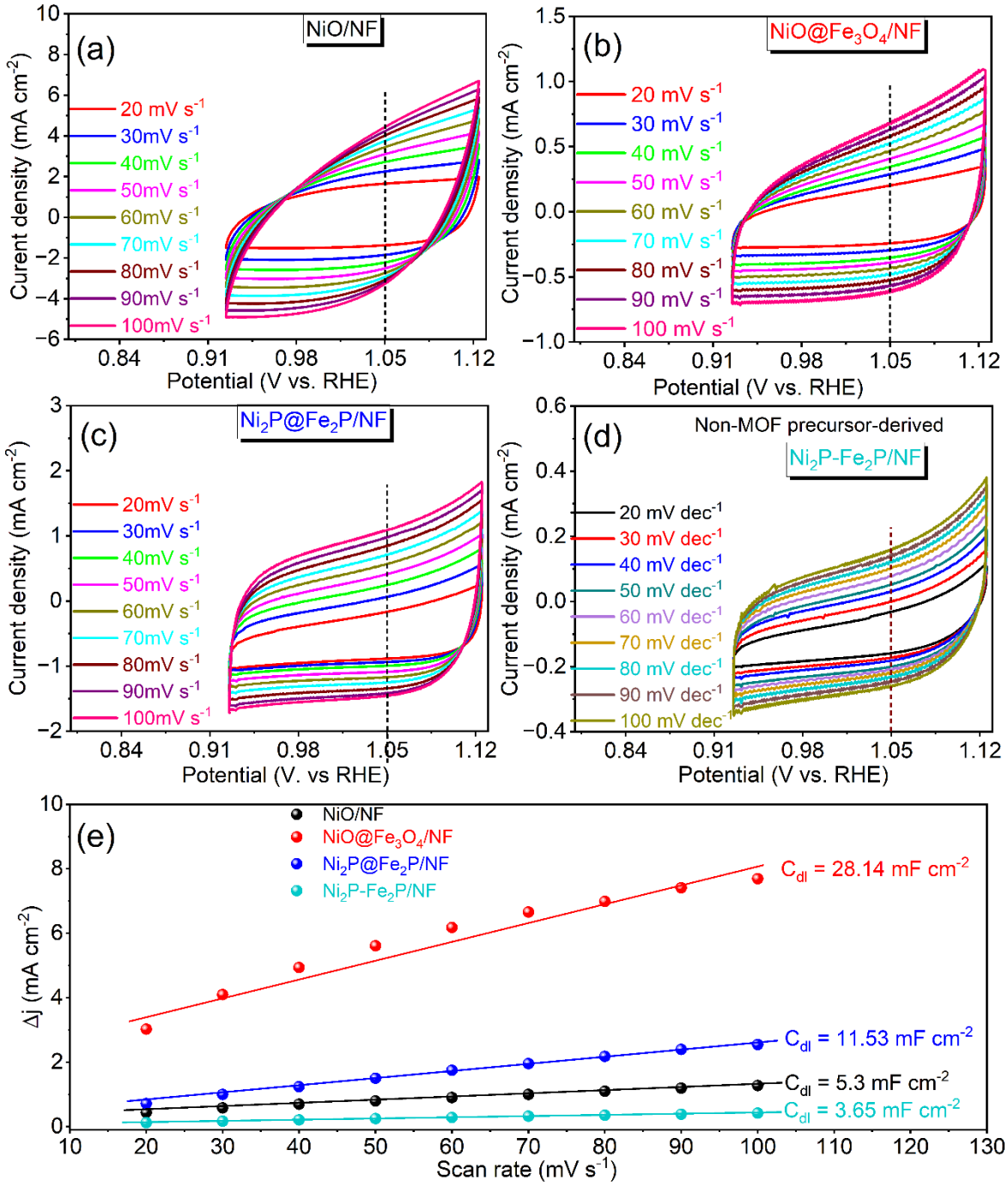

Fig. S2 Cyclic voltammograms at different scan rates of (a) NiO/NF, (b) NiO@Fe_3O_4/NF, (c) Ni_2P@Fe_2P/NF, (d) non-MOF precursor-derived Ni_2P-Fe_2P/NF, and (e) difference in anodic and cathodic current densities (Δj) vs. scan rate plots with C_{dl} value.

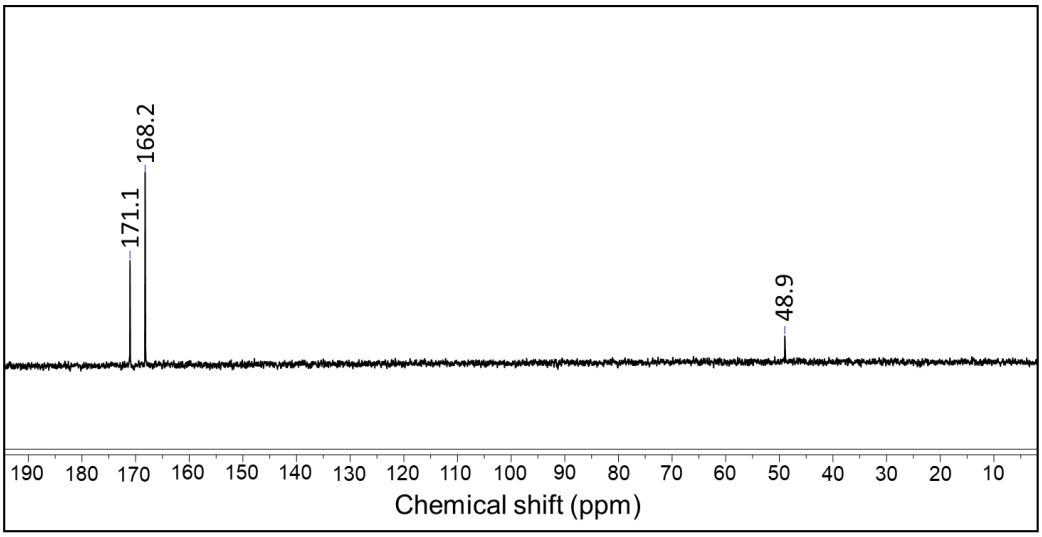

Fig. S3 ^{13}C-NMR of the 0.6 M MeOH + 1 M KOH electrolyte solution after MOR studies.

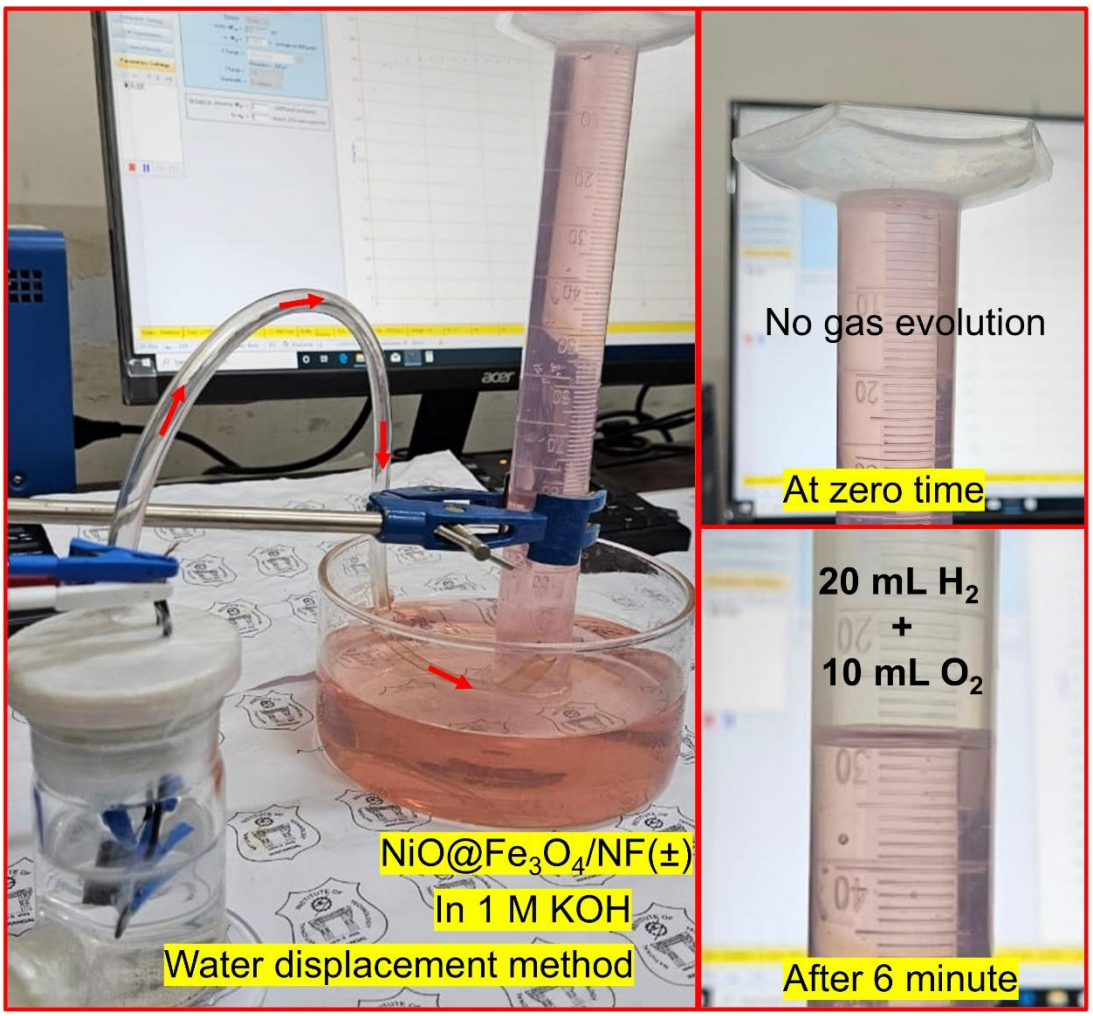

Fig. S4 Water displacement method for the conventional $NiO@Fe_3O_4/NF(\pm)$ electrolyzer to calculate Faradaic efficiency and H_2 production cost.

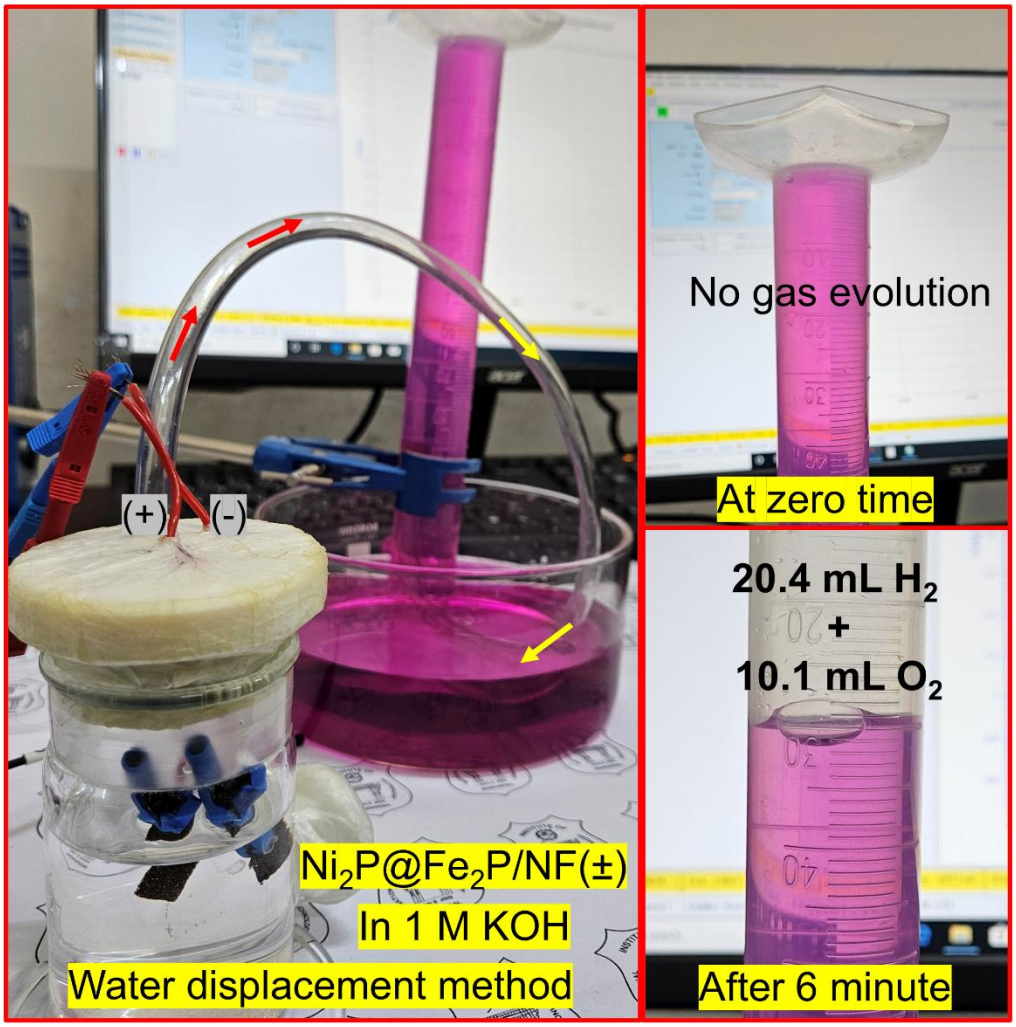

Fig. S5 Water displacement method for the conventional $Ni_2P@Fe_2P/NF(\pm)$ electrolyzer to calculate Faradaic efficiency and H_2 production cost.

Table S1 Comparison of OER activity of the studied electrocatalyst materials with recent results.

Electrocatalyst	Electrolyte	Current density ($mA\ cm^{-2}$)	η (mV vs. RHE)	Ref.
NiO/NF	1 M KOH	10	314	This work
		50	429	
		100	500	
$NiO@Fe_3O_4$/NF	1 M KOH	10	316	This work
		50	375	
		100	424	
$Ni_2P@Fe_2P$/NF	1 M KOH	10	210	This work
		50	268	
		100	317	
Mo-NiFeP/NIF	1 M KOH	10	207	S7
Mo-NiFeP/NIF	1 M KOH + seawater	10	257	S7
NiFeP@MXene	1 M KOH	10	240	S8
Ni_2P@MXene	1 M KOH	10	287	S8
ECO-NF-ACNT@NiFeP	1 M KOH	100	345	S9
NiSe@NiFe-LDH/NF	1 M KOH	10	209	S10
NiFeP/SG	1 M KOH	10	218	S11
CoS_x/Ni_3S_2@NF	1 M KOH	20	280	S12
FMCO/NF	1 M KOH	10	289	S13
CMO-1.25	1 M KOH	10	295	S14
FeCoMo/C	1 M KOH	10	330	S15

Fe–Co/Mo_2C@NCF	1 M KOH	10	277	S16
CoNi/NC-YS	1 M KOH	10	292	S17
FeOOH/Ni_3N	1 M KOH	10	244	S18
Ni–Fe LDH@NiCu	1 M KOH	10	218	S19
Fe-NF-500	1 M KOH	10	214	S20
Ni_2P-L/NF	1 M KOH	10	300	S21
c-CMO/PNF	1 M KOH	10	341	S22
Ni-EG-POR	1 M KOH	10	400	S23

Table S2 Comparison of MOR activity of Ni_2P@Fe_2P/NF electrocatalyst materials with recent results.

Electrocatalyst	**Electrolyte**	**Current density ($mA\ cm^{-2}$)**	**Potential (V vs. RHE)**	**Ref.**
Ni_2P@Fe_2P/NF	0.6 M MeOH + 1 M KOH	10	1.304	This work
		20	1.347	
		50	1.397	
		100	1.461	
Fe-NF-500	1 M MeOH + 1 M KOH	10	1.328	S20
c-CMO/PNF	1 M MeOH + 1 M KOH	10	1.393	S22
Ni-EG-POR	0.5 M MeOH + 1 M KOH	10	1.42	S23
$Ni_2Co_2Fe_1$-P	2 M MeOH + 1 M KOH	20	1.395	S24
$Co(OH)_2$@HOS/CP	3 M MeOH + 1 M KOH	10	1.385	S25

Ni-Co-Mo/CNFs	2 M MeOH + 1 M KOH	99.8	1.625	S26
$NiCo_2O_4/Ti_3C_2T_x$-MXene	0.5 M MeOH + 1 M KOH	~190	1.73	S27
$NiCo_2O_4/Ni(OH)_2$	0.5 M MeOH + 1 M KOH	92.3	1.63	S28
Ni50Co50-m	1.0 M MeOH + 1 M KOH	154	1.60	S29

Table S3 Comparison of HER activity of the studied electrocatalyst materials with recent results.

Electrocatalyst	**Electrolyte**	**Current density ($mA\ cm^{-2}$)**	***η*** **(mV vs. RHE)**	**Ref.**
NiO/NF	1 M KOH	−10	251	This work
		−50	389	
$NiO@Fe_3O_4$/NF	1 M KOH	−10	181	This work
		−50	311	
$Ni_2P@Fe_2P$/NF	1 M KOH	−10	124	This work
		−50	229	
		−100	297	
NiFeP@MXene	1 M KOH	−10	122	S8
Ni_2P@MXene	1 M KOH	−10	196	S8
ECO-NF-ACNT@NiFeP	1 M KOH	−100	348	S9
NiSe@NiFe-LDH/NF	1 M KOH	−10	93	S10

NiFeP/SG	1 M KOH	−10	115	S11
CoS_x/Ni_3S_2@NF	1 M KOH	−10	204	S12
c-CMO/PNF	1 M KOH	−10	130	S22
$Co(OH)_2$@HOS/CP	1 M KOH	−10	148	S25
Ni-Fe-P/NF	1 M KOH	−10	156	S30
NiFe NTAs-NF	1 M KOH	−10	181	S31
Ni-Co-P/NF	1 M KOH	−10	156	S32

Table S4 Comparison of OWE activity of the fabricated electrolyzers with recent results.

Electrocatalyst Anode (+)	**Electrocatalyst Cathode (-)**	**Electrolyte**	**Current density ($mA\ cm^{-2}$)**	**Cell voltage (V)**	**Ref.**
NiO/NF	NiO/NF	1 M KOH	10	1.775	This work
			50	2.060	
			100	2.223	
$NiO@Fe_3O_4$/NF	$NiO@Fe_3O_4$/NF	1 M KOH	10	1.679	This work
			50	1.862	
			100	1.988	
$Ni_2P@Fe_2P$/NF (OER)	$Ni_2P@Fe_2P$/NF (HER)	1 M KOH	10	1.464	This work
			20	1.570	
			50	1.717	
			100	1.838	
$Ni_2P@Fe_2P$/NF (MOR)	$Ni_2P@Fe_2P$/NF (HER)	1 M KOH + 0.6 M MeOH	10	1.458	This work
			20	1.517	
			50	1.605	

			100	1.702	
Mo-NiFeP/N	Mo-NiFeP/NIF	1 M KOH	10	1.55	S7
$(Ni_{0.75}Fe_{0.25})_2P$@MX ene	$(Ni_{0.75}Fe_{0.25})_2P$@MX ene	1 M KOH	10	1.64	S8
ECO-NF-ACNT@NiFeP	ECO-NF-ACNT@NiFeP	1 M KOH	20	1.53	S9
NiSe@NiFe-LDH/NF	NiSe@NiFe-LDH/NF	1 M KOH	10	1.56	S10
NiFeP/SG	NiFeP/SG	1 M KOH	10	1.54	S11
FeOOH/Ni_3N	FeOOH/Ni_3N	1 M KOH	10	1.58	S18
Ni–Fe LDH@NiCu	NiFeOx@NiCu	1 M KOH	10 50	1.523 1.736	S19
Fe-NF-500 (OER)	$MoNi_4$ (HER)	1 M KOH	10	1.516	S20
Fe-NF-500 (MOR)	$MoNi_4$ (HER)	1 M KOH + 1 M MeOH	10	1.381	S20
$Co(OH)_2$@HOS/CP (MOR)	$Co(OH)_2$@HOS/CP (HER)	3 M MeOH + 1 M KOH	10	1.497	S25
Ni-Fe-P/NF (Ethanol OR)	Ni-Fe-P/NF (HER)	1 M KOH + 1 M EtOH	10	1.53	S30
Ni-Fe-P/NF (OER)	Ni-Fe-P/NF (HER)	1 M KOH	10	1.66	S30
NiFe NTAs-NF	NiFe NTAs-NF	1 M KOH	10	1.62	S31
Ni-Co-S/NF	Ni-Co-P/NF	1 M KOH	20	1.57	S32
$FeNiP_x$/NF	$FeNiP_x$/NF	1 M KOH	10	1.53	S33

			50	1.74	
NiFeP/NF	NiMoP/NF	1 M KOH	10	1.57	S34
$NiCo_2S_4$/NiFeP/NF	$NiCo_2S_4$/NiFeP/NF	1 M KOH	10	1.56	S35
a-$Ni_{0.65}Fe_{0.35}(OH)_2$	a-$Ni_{0.65}Fe_{0.35}(OH)_2$	1 M KOH	10	1.60	S36

References

S1 G. Rajeshkhanna, T. I. Singh, N. H. Kim and J. H. Lee, *ACS Appl. Mater. Interfaces*, 2018, **10**, 42453–42468.

S2 A. Raveendran, M. Chandran and R. Dhanusuraman, *RSC Adv.*, 2023, **13**, 3843–3876.

S3 S. Shit, S. Chhetri, W. Jang, N. C. Murmu, H. Koo, P. Samanta and T. Kuila, *ACS Appl. Mater. Interfaces*, 2018, **10**, 27712–27722.

S4 A. Borah, N. Sumit, S. Palaniyappan and G. Rajeshkhanna, *Sustain. Energy Fuels*, 2024, **8**, 2265–2279.

S5 G. A. Gebreslase, M. V. Martínez-Huerta and M. J. Lázaro, *J. Energy Chem.*, 2022, **67**, 101–137.

S6 A. Borah, N. Pooja, R. Pawar and G. Rajeshkhanna, *J. Mater. Chem. A*, 2025, **13**, 7215–7227.

S7 Y. Wang, P. Yang, Y. Gong, D. Liu, S. Liu, W. Xiao, Z. Xiao, Z. Li, Z. Wu and L. Wang, *Chem. Eng. J.*, 2023, **468**, 143833.

S8 X. Zhang, D. Lin, R. Wan, Y. Wang, Q. Pan, F. Han, M. Li and B. Chen, *ACS Appl. Nano Mater.*, 2024, **7**, 7684–7693.

S9 X. Zhou, F. Fei, M. Li, X. Cao, X. Dong, L. Li, N. Yuan and J. Ding, *ACS Appl. Nano Mater.*, 2023, **6**, 8028–8035.

S10 W. Wu, B. Min, H. Li, F. Liu, M. Zheng, K. Ding, S. Lu and M. Liu, *React. Chem. Eng.*, 2023, **8**, 1711–1718.

S11 R. Q. Li, B. L. Wang, T. Gao, R. Zhang, C. Xu, X. Jiang, J. Zeng, Y. Bando, P. Hu, Y. Li and X. B. Wang, *Nano Energy*, 2019, **58**, 870–876.

S12 S. Shit, S. Chhetri, W. Jang, N. C. Murmu, H. Koo, P. Samanta and T. Kuila, *ACS Appl. Mater. Interfaces*, 2018, **10**, 27712–27722.

S13 W. Liu, W. Que, R. Yin, J. Dai, D. Zheng, J. Feng, X. Xu, F. Wu, W. Shi, X. Liu and X. Cao, *Appl. Catal. B Environ.*, 2023, **328**, 122488.

S14 R. Nadarajan, A. V. Gopinathan, N. P. Dileep, A. S. Sidharthan and M. M. Shaijumon, *Nanoscale*, 2023, **15**, 15219–15229.

S15 Y. Hou, W. Quan, Y. Lin, Z. Hong, R. Yang, H. Yao and Y. Huang, *Electrochim. Acta*, 2023, **463**, 142844.

S16 J. Hong, L. Zhang, Q. Zhu, Z. Du, Y. Zhou, T. Wågberg and G. Hu, *Mater. Horiz.*, 2023, **10**, 5969–5982.

S17 G. Hou, X. Jia, H. Kang, X. Qiao, Y. Liu, Y. Li, X. Wu and W. Qin, *Appl. Catal. B Environ.*, 2022, **315**, 121551.

S18 J. Guan, C. Li, J. Zhao, Y. Yang, W. Zhou, Y. Wang and G. R. Li, *Appl. Catal. B Environ.*, 2020, **269**, 118600.

S19 Y. Zhou, Z. Wang, Z. Pan, L. Liu, J. Xi, X. Luo and Y. Shen, *Adv. Mater.*, 2019, **31**, 1806769.

S20 Y. Hao, D. Yu, S. Zhu, C. H. Kuo, Y. M. Chang, L. Wang, H. Y. Chen, M. Shao and S. Peng, *Energy Environ. Sci.*, 2023, **16**, 1100–1110.

S21 C. Wang, L. Chai, X. Cui, Z. Zhou and S. Liu, *J. Phys. Chem. C*, 2021, **125**, 21443–21452.

S22 A. Sathyaseelan, S. Ramasamy, V. Elumalai, P. Kumar, N. U. H. L. Ali, P. Pazhamalai, T. D. Dongale, M. S. M. Saleem, M. Perumalsamy, A. A. Saj and S. J. Kim, *Appl. Catal. B Environ.*, 2024, **359**, 124472.

S23 S. N. Bhaduri, D. Ghosh, R. Chatterjee, S. Das, I. Pramanick, A. Bhaumik and P. Biswas, *Inorg. Chem.*, 2023, **62**, 12832–12842.

S24 J. Chang, W. Wang, D. Wu, F. Xu, K. Jiang, Y. Guo and Z. Gao, *J. Colloid Interface Sci.*, 2023, **648**, 259–269.

S25 K. Xiang, D. Wu, X. Deng, M. Li, S. Chen, P. Hao, X. Guo, J. L. Luo and X. Z. Fu, *Adv. Funct. Mater.*, 2020, **30**, 1909610.

S26 S. Awad, A. A. M. Al-Dies, R. Almahdawi, F. U. Y. Al-sheqefi and E. E. Abdel-Hady, *Polym. Adv. Technol.*, 2024, **35**, 6322.

S27 N. Narayanan, H. Liu, W. Zhang, B. Ravichandran, Q. Xu, L. Khotseng, Y. Cheng and H. Su, *ACS Appl. Nano Mater.*, 2024, **7**, 3907–3917.

S28 B. Wang, Y. Cao, Y. Chen, R. Wang, X. Wang, X. Lai, C. Xiao, J. Tu and S. Ding, *Inorg. Chem. Front.*, 2018, **5**, 172–182.

S29 Y. Qi, Y. Zhu, H. Jiang and C. Li, *Chin. J. Catal.*, 2024, **56**, 139–149.

S30 S. Sheng, Y. Song, L. Sha, K. Ye, K. Zhu, Y. Gao, J. Yan and G. Wang, *Appl. Surf. Sci.*, 2021, **561**, 150080.

S31 L. Xu, F. T. Zhang, J. H. Chen, X. Z. Fu, R. Sun and C. P. Wong, *ACS Appl. Energy Mater.*, 2018, **1**, 1210–1217.

S32 Y. Gong, Z. Xu, H. Pan, Y. Lin, Z. Yang and J. Wang, *J. Mater. Chem. A*, 2018, **6**, 12506–12514.

S33 C. Xiao, B. Zhang and D. Li, *Electrochim. Acta*, 2017, **242**, 260–267.

S34 H. Roh, H. Jung, H. Choi, J. W. Han, T. Park and S. Kim, *Appl. Catal. B Environ.*, 2021, **297**, 120434.

S35 J. Jiang, F. Li, H. Su, Y. Gao, N. Li and L. Ge, *Chin. Chem. Lett.*, 2022, **33**, 4367–4374.

S36 Y. Cheng, Z. Yin, W. M. Ma, Z. X. He, X. Yao and W. Y. Lv, *Inorg. Chem.*, 2022, **61**, 3327–3336.